

Accommodating scalar resonances in the HEFT

Iñigo Asiain,^{1,*} Domènec Espriu,^{1,†} and Federico Mescia^{1,2,‡}

¹*Departament de Física Quàntica i Astrofísica,*

Institut de Ciències del Cosmos (ICCUB),

Universitat de Barcelona, Martí Franquès 1, 08028 Barcelona, Spain

²*Istituto Nazionale di Fisica Nucleare, Laboratori Nazionali di Frascati,*

C.P. 13, 00044 Frascati, Italy

Loss of unitarity in an effective field theory is often cured by the appearance of dynamical resonances, revealing the presence of new degrees of freedom. These resonances may manifest themselves when suitable unitarization techniques are implemented in the effective theory, which in the scalar-isoscalar channel require using the coupled-channel formalism. Experimental detection of a resonance would provide precious information on the couplings and constants of the relevant effective theory. Conversely, the absence of a resonance where the unitarized effective theory predicts it should be allows us to rule out a certain range of couplings that would otherwise be allowed. Likewise, the appearance of unphysical (e.g. acausal) resonances is telling us that no UV completion could give rise to the corresponding couplings in the effective theory. In this talk we summarize the systematical procedure we have implemented in order to confront the effective theory with the absence or presence of resonances in the vector boson fusion channel at the LHC.

*Electronic address: iasaiain@icc.ub.edu

†Electronic address: espriu@icc.ub.edu

‡Electronic address: mescia@ub.edu

Contents

I. Introduction	1
II. The HEFT and the chiral parameter space	1
III. Unitarized partial waves	2
IV. Summary of the results	4
V. Main conclusions	8
References	9

I. INTRODUCTION

A clear indication of the existence of New Physics (NP) with strong interactions beyond-the-standard model (BSM) would be the appearance of unexpected resonances in the spectrum. A promising place to look for such resonances is in the electroweak symmetry breaking sector (EWSBS), consisting of the gauge bosons, their associated Goldstones and the Higgs boson, responsible for the generation of the masses of the elementary particles of the Standard Model (SM). While the general ideas behind the spontaneous symmetry breaking (SSB) mechanism seems well established, the nature of the Higgs and its interactions are not so obvious. In particular, the choice of the potential, built upon the principles of renormalizability and simplicity, is largely untested.

It is natural to look for NP in the EWSBS at the LHC is in vector boson fusion (VBF), and particularly in the interactions of the longitudinal components of the gauge bosons, as these are the ones intimately related to the SSB of the vacuum. This is perhaps best understood in the framework of the Equivalence Theorem (ET)[1], which states that at high energies compared to the electroweak scale, the longitudinal component of the gauge bosons can be substituted by their associated Goldstones. A throughout discussion of the ET and the error that one assumes with its usage can be found in Refs. [2, 3].

Here we summarize a systematical procedure to derive interesting phenomenological bounds on the coefficients of the Higgs potential, based on the properties of possible scalar resonances emerging in the context of a strongly interacting EWSBS.

II. THE HEFT AND THE CHIRAL PARAMETER SPACE

The Higgs effective field theory (HEFT) is a non-linear chiral Lagrangian describing the electroweak interactions up to the TeV scale that contains the Higgs boson as an $SU(2)$ singlet, in clear contrast to the linear case. The three Goldstones ω^a are included in a matrix exponential $U = \exp(i\omega^a\sigma^a/v)$ taking values in the coset $SU(2)_L \times SU(2)_R/SU(2)_V$.

We restrict ourselves to operators that respect the custodial symmetry, a limit in which the gauge bosons transform exactly as a triplet under the so-called custodial group. In our case, this limit is obtained by setting $g' = 0$, where g' is the gauge coupling associated to the abelian hypercharge group of the SM. This approximation seems justified by the ρ

parameter value [4].

Up to next-to-leading-order (NLO) we have the Lagrangian density

$$\mathcal{L}_2 = -\frac{1}{2g^2}\text{Tr}\left(\hat{W}_{\mu\nu}\hat{W}^{\mu\nu}\right) - \frac{1}{2g'^2}\text{Tr}\left(\hat{B}_{\mu\nu}\hat{B}^{\mu\nu}\right) + \frac{v^2}{4}\mathcal{F}(h)\text{Tr}\left(D^\mu U^\dagger D_\mu U\right) + \frac{1}{2}\partial_\mu h\partial^\mu h - V(h) \quad (1)$$

$$\begin{aligned} \mathcal{L}_4 = & -ia_3\text{Tr}\left(\hat{W}_{\mu\nu}[V^\mu, V^\nu]\right) + a_4(\text{Tr}(V_\mu V_\nu))^2 + a_5(\text{Tr}(V_\mu V^\mu))^2 + \frac{\gamma}{v^4}(\partial_\mu h\partial^\mu h)^2 \\ & + \frac{\delta}{v^2}(\partial_\mu h\partial^\mu h)\text{Tr}(D_\mu U^\dagger D^\mu U) + \frac{\eta}{v^2}(\partial_\mu h\partial_\nu h)\text{Tr}(D^\mu U^\dagger D^\nu U) \\ & + i\chi\text{Tr}\left(\hat{W}_{\mu\nu}V^\mu\right)\partial^\nu\mathcal{G}(h) \end{aligned} \quad (2)$$

with the usual vector structures $V_\mu = D_\mu U^\dagger U$, $\hat{W}_{\mu\nu} = \frac{1}{2}gW_\mu^a\sigma^a$, the \mathcal{F}, \mathcal{G} flare-functions and the parametrization of the Higgs potential

$$\begin{aligned} \mathcal{F}(h) &= 1 + 2a\frac{h}{v} + b\left(\frac{h}{v}\right)^2 + o(h/v)^3, \quad \mathcal{G}(h) = 1 + b_1\frac{h}{v} + o(h/v)^2 \\ V(h) &= \frac{1}{2}M_h^2 h^2 + d_3\lambda_{SM}vh^3 + d_4\frac{\lambda_{SM}}{4}h^4 + \dots \end{aligned} \quad (3)$$

All operators are sorted by the number of derivatives and soft mass scales. More information about this so-called *chiral counting* can be found in Ref. [5]. The coefficients accompanying these operators, in general different to their SM values, are referred to as *anomalous* couplings. One can easily recover the SM by setting all the anomalous couplings in \mathcal{L}_2 to 1, and the ones in \mathcal{L}_4 to zero, as they are absent in the SM. Table I collects all the relevant experimental bounds for the anomalous couplings up to date. The ones absent are not experimentally constrained at the moment.

With $\mathcal{L}_2+\mathcal{L}_4$, we obtain all the relevant $2 \rightarrow 2$ amplitudes $W_L W_L \rightarrow W_L W_L$, $W_L W_L \rightarrow hh$ and $hh \rightarrow hh$. Each of these three amplitudes up to NLO are decomposed in a tree-level contribution, obtained from $\mathcal{L}_2+\mathcal{L}_4$, and a one-loop contribution that for simplicity is derived using the ET containing only \mathcal{L}_2 interactions. The ultraviolet divergences from the one-loop calculation are absorbed by the proper redefinitions of the parameters of the Lagrangian. Detailed information about amplitudes and local counterterms is provided in Ref. [5].

III. UNITARIZED PARTIAL WAVES

The expansion in derivatives (momenta) typically leads to amplitudes that quickly violate unitarity, even for small departures from the SM values. In order to avoid this unphysical

Couplings	Ref.	Experiments
$0.89 < a < 1.13$	[6]	CMS (from $H \rightarrow VV$)
$0.55 < b < 1.49$	[7]	ATLAS (from $HH \rightarrow X$)
$-0.4 < d_3 < 6.3$	[8]	ATLAS (from $H \rightarrow X$ and $HH \rightarrow X$)
$-0.0061 < a_4 < 0.0063$	[9]	CMS (from $WZ \rightarrow 4l$)
$-0.0094 < a_5 < 0.0098$	[10]	CMS (from $WZ/WW \rightarrow 2l2j$)

TABLE I: Current experimental constraints on bosonic HEFT anomalous couplings at 95% CL. X stands for different combinations of l^+l^- , $b\bar{b}$ and $\gamma\gamma$ that can participate in the process of Higgs decays.

behavior that would irremediably lead to an overestimation of any NP signal, one must *unitarize* the amplitudes by means of some unitarization technique. Most of them are built in the language of partial-waves, where the unitarity condition acquires simple expressions. We are interested in the projection of the amplitudes into a specific channel with fixed isospin and spin (IJ). The isoscalar-scalar waves are obtained using

$$t_{00}^{(n)} = \frac{1}{64\pi} \int_1^1 d(\cos\theta) T_0^{(n)}(s, \cos\theta), \quad (4)$$

where $T_0^{(n)}$ is the amplitude with $I = 0$ for each of the $2 \rightarrow 2$ amplitudes at chiral order n , see Ref. [3].

The Inverse Amplitude Method (IAM), extensively used in low energy QCD, is the one chosen:

$$t_{IJ} \approx t_{IJ}^{(2)} + t_{IJ}^{(4)} + \dots, \quad t_{IJ}^{\text{IAM}} = t_{IJ}^{(2)} \left(t_{IJ}^{(2)} - t_{IJ}^{(4)} \right)^{-1} t_{IJ}^{(2)}. \quad (5)$$

For the case $IJ = 00$, Eq. (5) is applied in a matrix version containing all the possible processes that can participate in the channel at chiral order n :

$$t_{00}^{(n)} = \begin{pmatrix} t_{00}^{WW,(n)} & t_{00}^{Wh,(n)} \\ t_{00}^{Wh,(n)} & t_{00}^{hh,(n)} \end{pmatrix}, \quad (6)$$

where WW , Wh and hh indicate $W_L W_L \rightarrow W_L W_L$, $W_L W_L \rightarrow hh$ and $hh \rightarrow hh$, respectively. As all these amplitudes mix along the unitarization process when the Eq. (5) is applied, this method receives the name of coupled-channel formalism.

A scalar resonance, if present, appears in the spectrum as a pole of the unitarized wave t_{00}^{IAM} . Looking at Eq. (5), this occurs when $\det(t_{00}^{(2)}(s_R) - t_{00}^{(4)}(s_R)) = 0$ for a complex value of the Mandelstam variable $s_R = M_S^2 - \frac{i}{2}\Gamma_S M_S$, where M_S and Γ_S define the mass and width of the resonance. A resonance is considered physical when it appears on the second Riemann sheet of the complex s -plane, after analytical continuation across the physical cut in the real axis. Additionally, it must satisfy the condition $\Gamma < M/4$. Whenever an analytical continuation is not feasible due to the complexity of the amplitudes, the way we choose to determine whether a resonance is physical or not is by the phase-shift criterion: the phase δ (in the complex sense) of an amplitude that contains a physical resonance presents a shift from $\pi/2$ to $-\pi/2$ at the real pole position. A shift in the opposite direction is considered unphysical, due to $\Gamma^{-1} \sim \partial\delta(s)/\partial\sqrt{s}$.

IV. SUMMARY OF THE RESULTS

For this analysis we assume that any set of anomalous couplings leading to spurious resonances lacks a proper UV completion and cannot define a valid HEFT. Additionally, a scalar resonance lighter than 1.8 TeV should have already been observed, allowing us to rule out the corresponding set of anomalous couplings. This threshold is motivated by the study in Ref. [11], which constrains possible vector masses to $M_V \gtrsim 2$ TeV. Since experience suggests that scalar multiplets tend to be lighter than their vector counterparts, we adopt a slightly relaxed bound of 1.8 TeV.

Because the HEFT parameter space is large, it helps noticing a clear hierarchy between a_4 and a_5 (that have the largest number of derivatives) and the remaining couplings, even if nominally of the same chiral order. However it is worth checking the relevance of other operators, in particular those involving the propagation of the transverse gauge degrees of freedom inside the loops. A detailed discussion about their relative contributions can be found in Ref. [3]. For instance, in Table II we show the impact of going beyond the $g = 0$ case (the naive ET limit) for some specific benchmark points (BPs) for $a_4 - a_5$ in the limit $a = b^2$. The inclusion of transverse modes translates into heavier resonances by a difference of a 2 – 3%.

However, once one moves from the case $g = 0$ (i.e. the naive ET), the decoupling limit does not take place even for setting $a = b^2$, so a coupled-channel analysis is required for our

$\sqrt{s_S} (GeV)$	$a_4 \cdot 10^4$	$a_5 \cdot 10^4$	$g = 0$	$g \neq 0$
	1	-0.2	$1805 - \frac{i}{2}130$	$1856 - \frac{i}{2}125$
	2	-1	$2065 - \frac{i}{2}160$	$2119 - \frac{i}{2}150$
	3.5	-2	$2175 - \frac{i}{2}170$	$2231 - \frac{i}{2}163$

TABLE II: Values for the location of the scalar poles $\sqrt{s_S} = M_S - \frac{i}{2}\Gamma_S$ for $g = 0$ and $g \neq 0$ for some points in the $a_4 - a_5$ plane and in the decoupling limit $b = a^2$ within the nET with $a = b = 1$. All other couplings are set to the SM values. Note that the coupling to other $I = 0$ channels is ignored here for the purpose of assessing the effect of switching on the transverse modes.

study. This is shown Table II. One immediately notices in Table III is that when (correctly)

	$a_4 \cdot 10^4$	$a_5 \cdot 10^4$	S.C.	C.C.	$M_V - \frac{i}{2}\Gamma_V$
BP1	3.5	1	$1044 - \frac{i}{2}50$	$1844 - \frac{i}{2}487$	$2540 - \frac{i}{2}27$
BP2	-1	2.5	$1219 - \frac{i}{2}75$	$2156 - \frac{i}{2}637$	—
BP3	1	1	$1269 - \frac{i}{2}75$	$2244 - \frac{i}{2}675$	—

TABLE III: Properties of the scalar resonances for the selected benchmark points in the $a_4 - a_5$ plane, with the $\mathcal{O}(p^2)$ parameters set to their standard values, in both single-channel (S.C.) and coupled-channel (C.C.) formalism. We also include the values of the properties of vector resonances if present. The dots indicate the absence of a zero in the determinant. The $\mathcal{O}(p^2)$ chiral parameters are set to their SM values. We see that coupling channels modifies very substantially masses and widths. Poles not fulfilling the resonance condition are in boldface.

considering coupled channels, the results differ considerably from the ones obtained in single channel and the resonance masses and widths visibly increase. Recall that here we are assuming $a = b = 1$ where naively one would expect to have decoupling (this is the case in the nET), but this is not so because $g \neq 0$. In fact some of the would-be resonances even disappear as such by just becoming broad enhancements.

With respect to the vector case, where only a_4 and a_5 matters as they basically determine the position of the vector resonances, the HEFT parameter space to study scalar resonances is much larger, even after dropping a_3 and $\zeta \equiv b_1\chi$ from our analysis, as more processes are involved. Let us now proceed with the study in the cas $a = b = d_3 = d_4 = 1$ —the SM case

at LO—and assuming natural values for these extra NLO couplings—they do not exceed an absolute value of 10^{-3} . The following results for the position of the resonances are found for BPs where only scalar resonances—and no vector nor tensor—emerge

$M_S - \frac{i}{2}\Gamma_S$	$\gamma = 0$	$\gamma = 0.5 \cdot 10^{-4}$	$\gamma = 1 \cdot 10^{-4}$	$\gamma = -0.5 \cdot 10^{-4}$	$\gamma = -1 \cdot 10^{-4}$
BP1	1844 - $\frac{i}{2}$ 487	1668 - $\frac{i}{2}$ 212	1594 - $\frac{i}{2}$ 162	—	—
BP2	2156 - $\frac{i}{2}$ 637	1881 - $\frac{i}{2}$ 212	1781 - $\frac{i}{2}$ 162	—	—
BP3	2244 - $\frac{i}{2}$ 675	1931 - $\frac{i}{2}$ 200	1831 - $\frac{i}{2}$ 162	—	—

TABLE IV: Pole position for the benchmark points in Table III varying the $\mathcal{O}(p^4)$ parameter γ . The rest of the parameters are set to their SM values. Values in boldface indicate broad resonances that do not satisfy $\Gamma < M/4$.

$M_S - \frac{i}{2}\Gamma_S$	$\delta = 0$	$\delta = 0.5 \cdot 10^{-4}$	$\delta = 1 \cdot 10^{-4}$	$\delta = -0.5 \cdot 10^{-4}$	$\delta = -1 \cdot 10^{-4}$
BP1	1844 - $\frac{i}{2}$ 487	1744 - $\frac{i}{2}$ 362	1669 - $\frac{i}{2}$ 300	1994 - $\frac{i}{2}$ 1100	⊗
BP2	2156 - $\frac{i}{2}$ 637	1981 - $\frac{i}{2}$ 387	1869 - $\frac{i}{2}$ 300	2644 - $\frac{i}{2}\Gamma$	—
BP3	2244 - $\frac{i}{2}$ 675	2031 - $\frac{i}{2}$ 400	1906 - $\frac{i}{2}$ 287	—	—

TABLE V: Pole position for the benchmark points in Table III varying the $\mathcal{O}(p^4)$ parameter δ . The rest of the parameters are set to their SM values. Values in boldface indicate broad resonances that do not satisfy $\Gamma < M/4$. The symbols — and ⊗ are introduced to represent the absence of a zero in the determinant of the IAM matrix and the appearance of a second pole that is non-physical following the phase-shift criteria, respectively.

$M_S - \frac{i}{2}\Gamma_S$	$\eta = 0$	$\eta = 0.5 \cdot 10^{-4}$	$\eta = 1 \cdot 10^{-4}$	$\eta = -0.5 \cdot 10^{-4}$	$\eta = -1 \cdot 10^{-4}$
BP1	1844 - $\frac{i}{2}$ 487	1806 - $\frac{i}{2}$ 437	1769 - $\frac{i}{2}$ 387	1881 - $\frac{i}{2}$ 575	1931 - $\frac{i}{2}$ 712
BP2	2156 - $\frac{i}{2}$ 637	2094 - $\frac{i}{2}$ 512	2031 - $\frac{i}{2}$ 437	2256 - $\frac{i}{2}$ 887	2394 - $\frac{i}{2}\Gamma$
BP3	2244 - $\frac{i}{2}$ 675	2156 - $\frac{i}{2}$ 537	2094 - $\frac{i}{2}$ 450	2356 - $\frac{i}{2}$ 925	2544 - $\frac{i}{2}\Gamma$

TABLE VI: Pole position for the benchmark points in Table III varying the $\mathcal{O}(p^4)$ parameter η . The rest of the parameters are set to their SM values. Values in boldface indicate broad resonances that do not satisfy $\Gamma < M/4$.

From Tables IV-VI above we can see a different scenario from the one in the vector-

isovector case. The location of the pole changes 15% – 20% when we use reasonable values of γ and δ ($\sim 10^{-4}$) and softer variations of around 4% – 8% for values of η of the same order.

However, these results could be improved by studying the more general scenario where they are all non-zero. When studying the combined effect in the $\delta - \eta$ plane, we obtain the results in Figure 1. No matter the value of γ or the benchmark point selected, the presence of an unphysical pole leads us to exclude the parameter space above the bands. We also find that the greater the value of γ is, the more restriction we find (there are more excluded space above the band), especially for BP1. Below the bands, we find a nonresonant scenario.

Finally, one of the more interesting results of this systematic analysis comes from varying the couplings of the Higgs potential. In the case of the trilinear coupling of the Higgs potential d_3 , that now enters at tree level in the determination of the scalar resonances due to the mixing, we find that for $d_3 \gtrsim 2.5$ a second pole clearly appears (notation pole1 over pole2) in the low-energy region around ~ 1 TeV and it is also physical because it is found in the second Riemann sheet of the complex s plane. However, one of the physical poles is located at energy scales much lower than our preestablished bound of 1.8 TeV, so, in principle, the corresponding set of parameters should be discarded. The results are shown in Table VII. In fact, there are already hints of this first resonance at $d_3 = 1.7$. Different non-zero, but yet natural, values for γ do not alter the results significantly. For the case of d_4 , driving modifications in the quartic Higgs self-coupling, we can repeat the same analysis to find the results of Table VIII.

From Table VIII we can say that, if all the rest of parameters are set to their SM values, we could exclude values of $d_4 \gtrsim 2$ for BP2 and BP3 and BP1 would be excluded since these parameters lead to light resonances that should have already been seen. As always we assume (rightly or wrongly) that any scalar resonance above 1.8 TeV should have been observed. And as always, we also force the vector resonances, if present, to be heavier than that scale.

We do not find any physical resonant state with $M_S \gtrsim 1.8$ TeV and $d_4 \gtrsim 6$.

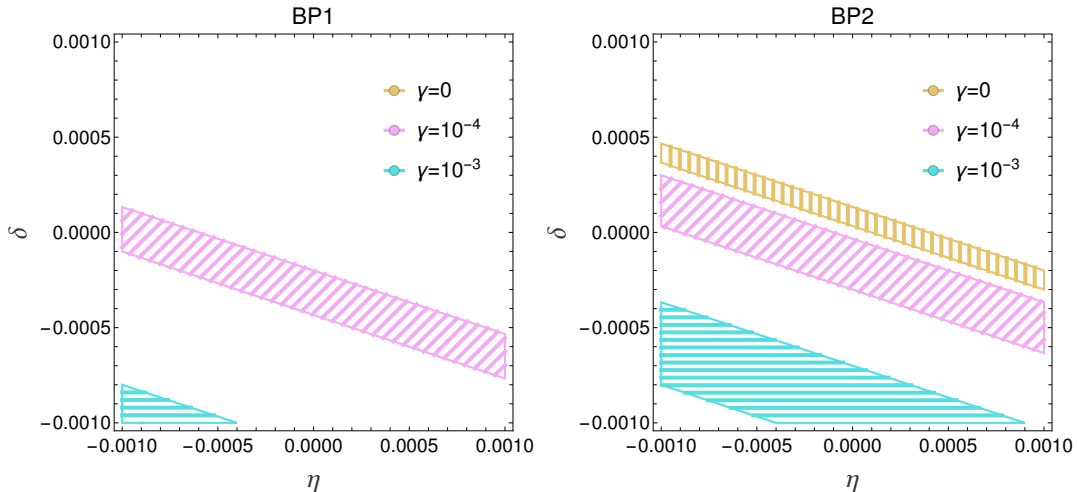


FIG. 1: Regions in the $\delta - \eta$ plane where physical resonances satisfying $M_S > 1.8$ TeV and for two of the benchmark points in Table III appear for different values of γ : $\gamma = 0$ (golden vertical lines), $\gamma = 10^{-4}$ (pink tilted lines) and $\gamma = 10^{-3}$ (blue horizontal lines). For all the values of γ , the region above the bands are excluded by the presence of a non-physical pole. Below the bands we find no resonances.

$M_S - \frac{i}{2}\Gamma_S$	$d_3 = 0.5$	$d_3 = 1$	$d_3 = 2$	$d_3 = 3$	$d_3 = 4$	$d_3 = 5$
BP1	$1769 - \frac{i}{2}275$	$1668 - \frac{i}{2}212$	$1544 - \frac{i}{2}112$	$994 - \frac{i}{2}23$ $1569 - \frac{i}{2}25$	$1044 - \frac{i}{2}37$ $1769 - \frac{i}{2}34$	$994 - \frac{i}{2}27$ $1994 - \frac{i}{2}54$
BP2	$1981 - \frac{i}{2}262$	$1881 - \frac{i}{2}212$	$1719 - \frac{i}{2}125$	$1106 - \frac{i}{2}27$ $1656 - \frac{i}{2}50$	$1219 - \frac{i}{2}37$ $1781 - \frac{i}{2}34$	$1118 - \frac{i}{2}26$ $1994 - \frac{i}{2}50$
BP3	$2031 - \frac{i}{2}250$	$1931 - \frac{i}{2}200$	$1769 - \frac{i}{2}125$	$1131 - \frac{i}{2}37$ $1681 - \frac{i}{2}38$	$1269 - \frac{i}{2}37$ $1781 - \frac{i}{2}27$	$1231 - \frac{i}{2}23$ $1994 - \frac{i}{2}53$

TABLE VII: Values of the pole position of the benchmark points in Table III with $\gamma = 0.5 \cdot 10^{-4}$ changing d_3 . The rest of the parameters are set to their SM values. The cells with two complex numbers indicate the pole position of the two physical Breit-Wigner poles in the denominator of the unitarized amplitude.

V. MAIN CONCLUSIONS

We have presented a systematical analysis to set bounds on HEFT coefficients describing the low-energy regime of a high-energy theory with strong interactions. By making use of

$M_S - \frac{i}{2}\Gamma_S$	$d_4 = 0.5$	$d_4 = 1$	$d_4 = 2$	$d_4 = 3$	$d_4 = 4$	$d_4 = 5$	$d_4 = 8$
BP1	$1794 - \frac{i}{2}250$	$1668 - \frac{i}{2}212$	$1494 - \frac{i}{2}137$	$1381 - \frac{i}{2}112$	$1306 - \frac{i}{2}87$	$1256 - \frac{i}{2}75$	$1169 - \frac{i}{2}50$
BP2	$1981 - \frac{i}{2}225$	$1881 - \frac{i}{2}212$	$1719 - \frac{i}{2}175$	$1606 - \frac{i}{2}125$	$1531 - \frac{i}{2}112$	$1481 - \frac{i}{2}87$	$1381 - \frac{i}{2}75$
BP3	$2031 - \frac{i}{2}225$	$1931 - \frac{i}{2}200$	$1781 - \frac{i}{2}162$	$1669 - \frac{i}{2}137$	$1594 - \frac{i}{2}112$	$1544 - \frac{i}{2}100$	$1444 - \frac{i}{2}75$

TABLE VIII: Values of the pole position of the benchmark points in Table III changing d_4 with $\gamma = 0.5 \cdot 10^{-4}$. The rest of the parameters are set to their SM values.

the partial wave analysis and unitarization techniques herein presented, and under some mild assumptions, we have been able to set bounds on the anomalous self-interactions of the Higgs pointing in the same direction that the experimental results: in particular we find $d_3 < 2$ and $d_4 < 2.5$.

The possibility of light scalar resonances, below our self-imposed limit $M_S < 1.8$ TeV, remains a logical possibility to be further studied. However, preliminary studies of a putative resonance at 650 GeV [12] place such possibility in a corner of parameter space and requires the concurrence of several parameters[13].

In conclusion, somewhat unexpectedly, the study of possible scalar resonances in WW fusion places very interesting restrictions on the space of Higgs couplings, a region that is hard to experimentally study. We have presented here some, we believe, relevant results, but certainly this line of research deserves further analysis.

-
- [1] J. M. Cornwall, D. N. Levin, and G. Tiktopoulos, Phys. Rev. D **10**, 1145 (1974), [Erratum: Phys.Rev.D 11, 972 (1975)].
- [2] D. Espriu and J. Matias, Phys. Rev. D **52**, 6530 (1995), hep-ph/9501279.
- [3] I. Asiáin, D. Espriu, and F. Mescia, Phys. Rev. D **107**, 115005 (2023), 2301.13030.
- [4] D. Ross and M. Veltman, Nuclear Physics B **95**, 135 (1975), ISSN 0550-3213, URL <https://www.sciencedirect.com/science/article/pii/055032137590485X>.
- [5] I. Asiáin, D. Espriu, and F. Mescia, Phys. Rev. D **105**, 015009 (2022), 2109.02673.
- [6] J. de Blas, O. Eberhardt, and C. Krause, JHEP **07**, 048 (2018), 1803.00939.
- [7] A. Hayrapetyan et al. (CMS), JHEP **10**, 061 (2024), 2404.08462.

- [8] G. Aad et al. (ATLAS), Phys. Lett. B **843**, 137745 (2023), 2211.01216.
- [9] A. M. Sirunyan et al. (CMS), Phys. Lett. B **795**, 281 (2019), 1901.04060.
- [10] A. M. Sirunyan et al. (CMS), Phys. Lett. B **798**, 134985 (2019), 1905.07445.
- [11] I. Rosell, A. Pich, and J. J. Sanz-Cillero, PoS **ICHEP2020**, 077 (2021), 2010.08271.
- [12] A. Kundu, A. Le Yaouanc, P. Mondal, and F. Richard, in *2022 ECFA Workshop on e+e- Higgs/EW/Top factories* (2022), 2211.11723.
- [13] I. Asiáin, D. Espriu, and F. Mescia, Phys. Rev. D **108**, 055013 (2023), 2305.03622.